Available online at www.sciencedirect.com
ScienceDirect
Journal of Catalysis 243 (2006) 229–238
JOURNAL OF CATALYSIS
www.elsevier.com/locate/jcat

# Flame-derived Pt/Ba/$Ce_xZr_{1-x}O_2$: Influence of support on thermal deterioration and behavior as $NO_x$ storage-reduction catalysts

Reto Strobel [a,b], Frank Krumeich [c], Sotiris E. Pratsinis [a], Alfons Baiker [b,*]

[a] *Particle Technology Laboratory, Department of Mechanical and Process Engineering, ETH Zurich, Sonneggstrasse 3, CH-8092 Zurich, Switzerland*
[b] *Institute for Chemical and Bioengineering, Department of Chemistry and Applied Biosciences, ETH Zurich, Wolfgang-Pauli-Strasse 10, CH-8093 Zurich, Switzerland*
[c] *Laboratory of Inorganic Chemistry, Department of Chemistry and Applied Biosciences, ETH Zurich, Wolfgang-Pauli-Strasse 10, CH-8093 Zurich, Switzerland*

Received 11 April 2006; revised 13 July 2006; accepted 14 July 2006

Available online 7 September 2006

**Abstract**

Pt/Ba catalysts for $NO_x$ storage-reduction (NSR) supported on ceria/zirconia were prepared by two-nozzle flame spray pyrolysis. Emphasis was placed on the effect of the support composition on the thermal deterioration and the related behavior during $NO_x$ storage and reduction. The materials were characterized by X-ray diffraction (XRD), nitrogen adsorption (BET), electron microscopy (TEM), and temperature-programmed decomposition (TPD). The as-prepared material consisted of intimately mixed agglomerates of $BaCO_3$ and $Ce_xZr_{1-x}O_2$ particles. Low thermal stability of $BaCO_3$ resulted in high $NO_x$ storage capacity. The support composition ($Ce_xZr_{1-x}O_2$) strongly affected the $NO_x$ reduction activity of Pt. Higher Ce content favored the formation of stable Pt oxides exhibiting lower reduction activity. Thermal deterioration was investigated in different atmospheres. At 800 °C, $BaCO_3$ transformed into inactive Ba zirconate and Ba cerate. At high Ce content, $BaCO_3$ was reformed when exposed to $CO_2$ at high temperatures, recovering its high $NO_x$ storage capacity. During the high-temperature treatment, however, Pt strongly deactivated, resulting in a loss of the catalyst's $NO_x$ reduction activity.


*Keywords:* $NO_x$ storage-reduction; Ceria/zirconia; Pt/Ba/$Ce_xZr_{1-x}O_2$; Platinum; Barium carbonate; Flame synthesis; Thermal deterioration; Barium zirconate; Barium cerate

## 1. Introduction

Lean-burn engines operating at high air-to-fuel ratios are a promising concept to comply with stricter regulations regarding fuel consumption of automotive engines. However, neither conventional three-way catalysts nor diesel exhaust catalysts are capable of reducing $NO_x$ emissions to acceptable levels under lean conditions. $NO_x$ storage-reduction (NSR) catalysts are the most promising concept for reducing $NO_x$ under lean conditions [1–3]. In general, NSR catalysts consist of a noble metal (Pt, Pd, or Rh) for oxidation and reduction of $NO_x$ and of a storage compound (typically containing Ba or K) to store $NO_x$ species in the form of nitrates under lean conditions. During short rich periods, $NO_2$ is released and reduced to $N_2$ over the noble metal [2–5]. The two components are supported on a thermally stable carrier material, typically $Al_2O_3$.

The major drawback of NSR catalysts is the high sensitivity to sulfur poisoning and the related deterioration during regeneration, resulting in steady deactivation of the catalyst [3,6–10]. This is attributed mainly to the formation of sulfates with the support and especially with the storage compound (i.e., $BaSO_4$) [10–12]. These sulfates are much more stable than the corresponding nitrates, and high temperatures (800 °C) are required to decompose the sulfates and regenerate an active storage material [11,12]. At these temperatures, thermal deterioration occurs by particle growth, loss of surface area, and especially formation of mixed oxides between the storage compound and materials from the support or washcoat (i.e., $BaAl_2O_4$). In general, the formation of such mixed oxides reduces the catalyst's $NO_x$ storage capacity. Two strategies have been proposed to

* Corresponding author. Fax: +41 44 632 1163.
*E-mail address:* baiker@chem.ethz.ch (A. Baiker).

0021-9517/$ – see front matter 
doi:10.1016/j.jcat.2006.07.016

solve these problems: (i) the development of catalysts that can be regenerated at lower temperatures, preventing the formation of $BaAl_2O_4$ [6,13,14], and (ii) the use of supporting materials that either do not form any mixed oxides with the storage material or form mixed oxides that easily decompose with in the presence of $CO_2$ or $NO_x$ [15]. Recently it has been shown that after formation of barium cerate ($BaCeO_3$), $BaCO_3$ and $CeO_2$ can be easily regenerated in a $CO_2$-containing atmosphere [15].

Here, the second strategy is explored, namely, the influence of support of Pt/Ba/$Ce_xZr_{1-x}O_2$ ($x = 0$–1) catalysts on thermal behavior and $NO_x$ storage-reduction activity. The ceria/zirconia-supported Pt/Ba NSR catalysts were prepared by two-nozzle flame-spray synthesis as already applied for synthesis of Pt/Ba/$Al_2O_3$ NSR-catalysts exhibiting good NSR activity [16,17]. The use of two nozzles prevents the formation of Ba containing mixed oxides and results in individual but well-mixed $BaCO_3$ and support particles. The fast $NO_x$ uptake of flame-made Pt/Ba/$Al_2O_3$ was attributed to the low thermal stability of the $BaCO_3$ in the flame-made catalysts. Flame-spray pyrolysis (FSP) has already been applied for synthesis of Pt/$Al_2O_3$ [18] and Pt/$Ce_xZr_{1-x}O_2$ [19] catalysts. Flame-made ceria/zirconia nanoparticles exhibit an almost ideal atomic mixing of Ce and Zr (solid solution) and very high thermal stability [19–21]. The unique ability of ceria to store and release $O_2$ makes automotive three-way catalysts (TWCs) the most important application of ceria, especially zirconia-stabilized ceria [22]. However, only few studies have investigated the applicability of $CeO_2$ and $Ce_xZr_{1-x}O_2$ as support materials for NSR catalysts [23–25].

## 2. Experimental

### 2.1. Apparatus and preparation

The Pt/Ba/$Ce_xZr_{1-x}O_2$ catalysts were prepared by two-nozzle FSP [16]. The Ce–Zr precursor solution consisted of cerium 2-ethylhexanoate (Alfa Aesar, 49% in 2-ethylhexanoic acid) and zirconium 2-ethylhexanoate (Alfa Aesar, >96%) dissolved in a 1:1 mixture of 2-ethylhexanoic acid (Fluka, >98%) and toluene (Riedel-de Haën, >99.5%) [21]. The total metal concentration (Ce + Zr) in this solution was always 0.2 mol/L. For the Pt/Ba-containing solution, corresponding amounts of barium 2-ethylhexanoate (Alfa Aesar, 75% in 2-ethylhexanoic acid) and platinum acetylacetonate (Strem, 98%) were dissolved in toluene. The setup consisted of two separate FSP nozzles. The angle between the two nozzles was 120°, and the distance between the angle tip and each nozzle center was 6 cm [16].

The individual spray nozzle has been described in detail previously [26]. The Ce–Zr precursor solution was fed at 5 ml/min through the first nozzle, and the Pt/Ba precursor solution was fed at 3 ml/min through the second nozzle. Each solution was dispersed by 5 L/min of oxygen (PanGas, 99.95%), forming two fine sprays. Both sprays were surrounded and ignited by a small flame ring issuing from an annular gap (0.15 mm spacing, 6 mm radius). The gas flow rates of these two individually premixed methane/oxygen supporting flames were 3.5 L/min each, with a $CH_4/O_2$ ratio of 0.46. Product particles were collected on a glass fiber filter (Whatman GF/D, 25.7 cm in diameter) with the aid of a vacuum pump (Busch, Seco SV 1040C). The nominal Pt:Ba:$Ce_xZr_{1-x}O_2$ weight ratio was always 1:20:100. Assuming that all Ba was present in the form of $BaCO_3$, the nominal Ba content was 15.4 wt%.

For comparison, $Al_2O_3$-supported catalysts have been prepared by two-nozzle FSP as reported earlier [16,17] and by incipient wetness impregnation [17,27]. The nominal Pt:Ba:$Al_2O_3$ weight ratio of these two materials was also 1:20:100. Detailed description of the experimental parameters together with a thorough comparison of the structural and catalytic properties of these flame-made and impregnated Pt/Ba/$Al_2O_3$ catalysts can be found elsewhere [17].

### 2.2. Characterization

The specific surface area (SSA) was determined by nitrogen adsorption at 77 K using the BET method (Micromeritics Tristar). Before analysis, samples were outgassed for 1 h in $N_2$ at 150 °C. The powder X-ray diffraction (XRD) patterns were recorded with a Bruker D8 advance diffractometer in step mode ($2\theta = 15°$–$75°$) with a step size of 0.04° and a scan speed of 0.48°/min. Temperature-programmed decomposition (TPD) of $BaCO_3$ was measured using a Micromeritics Autochem II 2920 by heating (10 °C/min) 35 mg of powder in a helium flow (20 ml/min) from 50 to 1000 °C. Gas-phase composition was monitored by a mass spectrometer (Thermostar, Pfeiffer Vacuum). After each experiment, the $CO_2$ signal ($M/Z = 44$) was calibrated by injecting a well-defined pulse of $CO_2$ (0.35 ml).

For transmission electron microscopy (TEM), the material was dispersed in ethanol and deposited onto a perforated carbon foil supported on a copper grid. The investigations were performed on a Tecnai F30 microscope (FEI, Eindhoven, with a field emission cathode, operated at 300 kV). TEM images were recorded with a slow-scan CCD camera. An energy filter (Gatan imaging filter [GIF]) installed below the Tecnai F30 allowed the recording of element-specific images (elemental maps) of Zr (180 eV), Ba (790 eV), and Ce (890 eV) by the electron spectroscopic imaging (ESI) technique [28].

Thermal stability was studied by annealing the catalysts at 800 °C for 2 h in air or for 1 h in 10% $O_2$/He, followed by 1 h in 20% $CO_2$/He. The heating and cooling rates were ±10 °C/min.

The NSR measurements were performed with 20 mg of catalyst in a fixed-bed reactor ($d = 4$ mm). The reactor was connected to a valve device, which allows rapid switching between oxidizing and reducing atmospheres. The NO and $NO_2$ concentrations in the effluent gas were monitored by a chemiluminescence detector (ECO Physics, CLD 822 S), and other gases were analyzed using a mass spectrometer (Thermostar, Pfeiffer Vacuum). The $NO_x$ conversion was derived from the corresponding $NO_x$ outlet concentration according to the following formula: $NO_x$ conversion $= (NO_{in} - NO_{x,out})/NO_{in} \times 100\%$.

The NSR was measured at 300, 350, and 400 °C by switching 5 times between oxidizing (3 min in 667 ppm NO and 6.67% $O_2$ in He) and reducing atmospheres (1 min in 667 ppm NO, 1333 ppm $C_3H_6$ in He). The total gas flow rate was al-

ways 60 ml/min. At the end of each experiment, the catalyst was kept under reducing conditions for 10 min, followed by oxidizing conditions until its saturation. For some experiments, catalysts were pretreated in 5% $H_2$/Ar at 500 °C for 30 min. In addition, some catalysts were directly exposed to lean conditions until saturation (90 min), followed by a rich phase for 45 min with no previous cycles.

## 3. Results and discussion

### 3.1. Structural properties

Two-nozzle FSP of Pt/Ba/$Ce_xZr_{1-x}O_2$ resulted in well-mixed but individual $BaCO_3$ and $Ce_xZr_{1-x}O_2$ nanoparticles. Fig. 1 shows TEM images with the corresponding Ba, Ce, and Zr elemental mappings for the as-prepared materials with different $Ce_xZr_{1-x}O_2$ compositions. It clearly shows that $BaCO_3$ particles are intimately mixed with the $Ce_xZr_{1-x}O_2$ particles. The ratio of Ce:Zr in the supporting material had hardly any influence on the morphology of the Ba component, which was similar to Pt/Ba/$Al_2O_3$ prepared by two-nozzle FSP [16,17]. Thus, it can be expected that $BaCO_3$ and $Ce_xZr_{1-x}O_2$ form separately before the two flames are mixed [16].

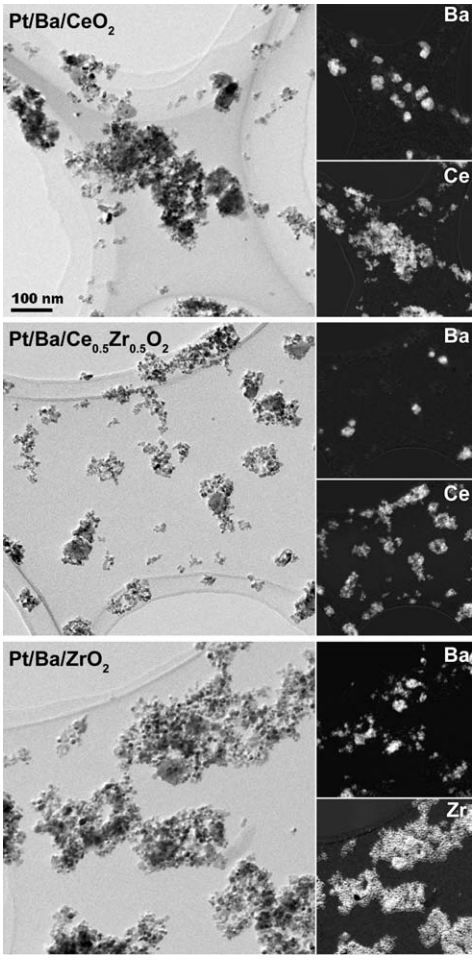


Fig. 1. TEM images of as-prepared Pt/Ba/$Ce_xZr_{1-x}O_2$ with the corresponding elemental mappings of Ba and Ce or Zr on the right.

Fig. 2 depicts XRD patterns of the as-prepared materials. Without the presence of Zr, ceria crystallized in its cubic crystal structure [20,26], while tetragonal zirconia was formed without Ce [29]. Fast cooling rates during preparation prevent the transformation into monoclinic $ZrO_2$ and favor the formation of tetragonal $ZrO_2$, the high-temperature form of zirconia. Crystalline (tetragonal) solid solutions of Ce and Zr were formed for Ce–Zr mixed oxides [20,21]. The addition of Ba and Pt did not influence the phase composition of the support. Barium was in the form of crystalline $BaCO_3$, and no crystalline BaO was observed [30]. For Ce:Zr ratios $>1$, only orthorhombic $BaCO_3$ was found (Figs. 2A and 2B). However, with more Zr present, Ba was mainly in the form of monoclinic $BaCO_3$ (Fig. 2C), which was formed during rapid quenching and gradually transformed into orthorhombic $BaCO_3$ when stored at ambient conditions [30,31]. For $Ce_{0.1}Zr_{0.9}O_2$, this transformation took place within 5 days, whereas on $ZrO_2$ it took about 1 month. This suggests that $ZrO_2$ stabilizes the metastable monoclinic form of $BaCO_3$ similar to $Al_2O_3$ [16].

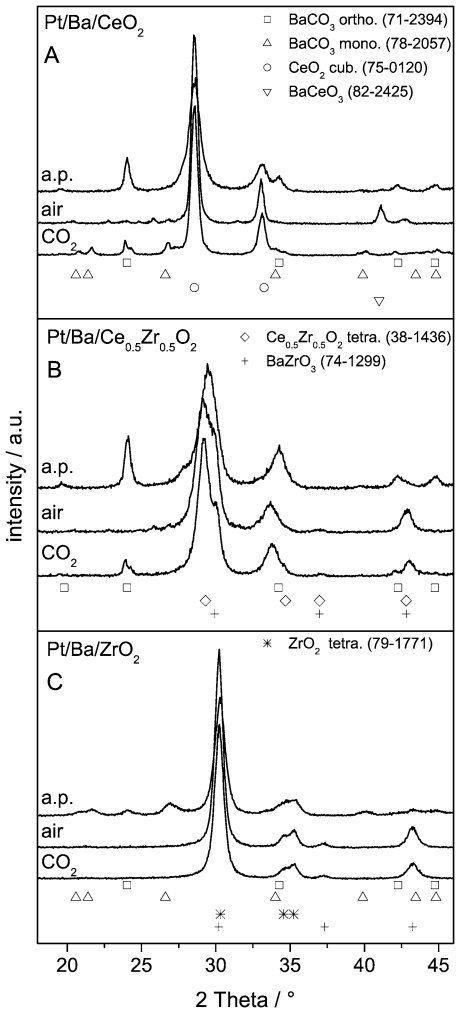


Fig. 2. X-ray diffraction patterns of Pt/Ba/$Ce_xZr_{1-x}O_2$ with different support composition: (a.p.) as-prepared; (air) after 2 h, 800 °C in air; ($CO_2$) after 1 h, 800 °C in 10% $O_2$/He followed by 1 h, 800 °C in 20% $CO_2$/He. JSPDS numbers of the corresponding crystal structures are shown in parenthesis.

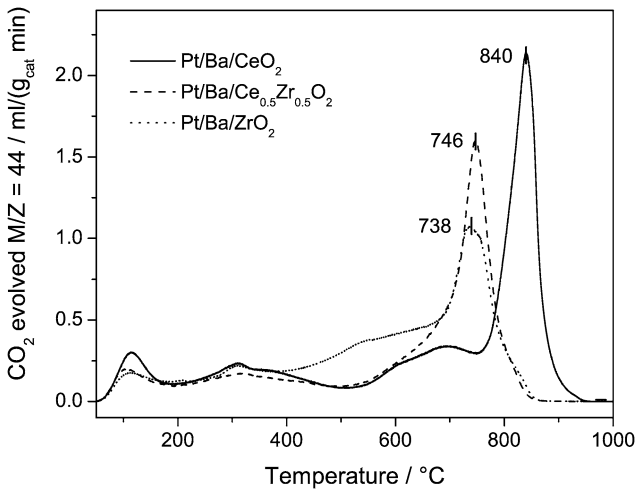


Fig. 3. TPD $CO_2$ evolution profiles during decomposition of $BaCO_3$ for as-prepared Pt/Ba/$Ce_xZr_{1-x}O_2$ with different support composition. Temperatures of maximum decomposition rate are indicated.

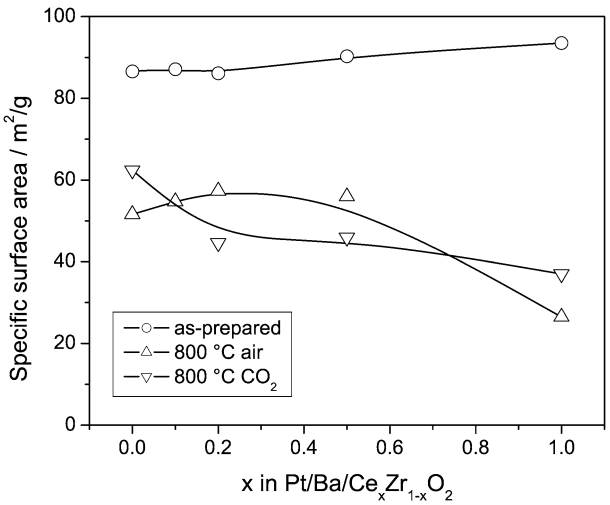


Fig. 4. Specific surface area of flame made Pt/Ba/$Ce_xZr_{1-x}O_2$ as a function of the support composition before and after annealing at 800 °C in air (air, 2 h) or in $CO_2$ containing atmosphere (10% $O_2$/He, 1 h followed by 20% $CO_2$/He, 1 h).

TPD of $BaCO_3$ in inert atmosphere was monitored by the evolution of $CO_2$ ($M/Z = 44$) and is shown in Fig. 3 for as-prepared materials. The evolution of $CO_2$ below 500 °C can be attributed mainly to desorption of surface-bound $CO_2$ species. The main peak between 600 and 900 °C originates from the decomposition of $BaCO_3$ into BaO and $CO_2$. Note that decomposition of $BaCO_3$ is most likely accompanied by formation of $BaZrO_3$ and $BaCeO_3$ (see Fig. 2). These decomposition temperatures are much lower than that of bulk-$BaCO_3$ (>900 °C) [27].

This low stability can be attributed to the close interaction of $BaCO_3$ with the support and has also been observed for flame-made [16] and impregnated [27] Ba on $Al_2O_3$. However, the decomposition temperatures of $BaCO_3$ in flame-made Pt/Ba/$Ce_xZr_{1-x}O_2$ are much lower than those reported for impregnated Pt/Ba on $CeO_2$ [15] and $ZrO_2$ [32]. On $CeO_2$, two kinds of $BaCO_3$ have been reported with maximum decomposition rates at 874 and 1100 °C [15,23]. In contrast, the corresponding flame-made material contained only $BaCO_3$ decomposing at low temperature (840 °C). Similar for Pt/Ba/$ZrO_2$: Two kinds of $BaCO_3$ were reported for impregnated catalysts ($T_d$ = ca. 750 °C and mainly 1000 °C [32]), whereas $BaCO_3$ decomposed completely at 738 °C on flame-made $ZrO_2$. These observations are in line with earlier results for flame-made and impregnated Pt/Ba/$Al_2O_3$ catalysts [17]. In any case, the flame-made $BaCO_3$ decomposes at lower temperatures than that present in the corresponding impregnated catalyst. The lower thermal stability of the flame-derived $BaCO_3$ could be caused by several factors, of which different structural properties of $BaCO_3$ and smaller particle size in flame-made catalysts, and strong interfacial contact between support and $BaCO_3$, promoting $BaCO_3$ decomposition and/or formation of Ba mixed oxides, are probably the most crucial.

The specific surface area of as-prepared and annealed (air, 800 °C, 2 h or with additional $CO_2$ treatment) catalysts is shown in Fig. 4. For as-prepared materials it was around 90 $m^2/g$ and increased slightly with higher ceria content. The strongest sintering at 800 °C was observed for $CeO_2$ (26 $m^2/g$), which is not surprising, because Zr is commonly used as a stabilizer for ceria. $ZrO_2$ and Ce–Zr mixed oxides retained a surface area of 50–60 $m^2/g$ after annealing [33]. For all materials, $BaCO_3$ decomposed during the high-temperature treatment in air, and the corresponding Ba-cerate ($BaCeO_3$) or zirconate ($BaZrO_3$) was formed, as shown in Fig. 2. With both Zr and Ce present in the support, only $BaZrO_3$ and no $BaCeO_3$ could be observed. This also results in Ce enrichment in the ceria/zirconia solid solution, as confirmed by a shift of the $Ce_{0.5}Zr_{0.5}O_2$ peaks toward lower diffraction angles [20,33].

The reformation of $BaCO_3$ in $CO_2$-containing atmosphere after decomposition and $BaCeO_3$ formation [15] was investigated by annealing the powders for 1 h at 800 °C in 10% $O_2$/He, followed by 20% $CO_2$/He for another 1 h at 800 °C and cooling to room temperature at 10 °C/min. XRD patterns recorded after this annealing procedure are shown in Fig. 2; the corresponding specific surface area is shown in Fig. 4. The $BaCO_3$ (orthorhombic and monoclinic) was easily reformed from $BaCeO_3$ (Fig. 2A, air, $CO_2$). Note that larger $BaCO_3$ crystallites were formed after this treatment compared with the as-prepared powder, as indicated by sharper reflections in the $BaCO_3$ crystal pattern (Fig. 2A, $CO_2$). Similar behavior was observed for Pt/Ba/$Ce_{0.5}Zr_{0.5}O_2$; however, less $BaCO_3$ was reformed, and crystalline $BaZrO_3$ was (although less prominent) still present (Fig. 2B, $CO_2$). This indicates that $BaZrO_3$ partly decomposes during $CO_2$ treatment when Ce is present in the support. In contrast, for Pt/Ba/$ZrO_2$, the additional $CO_2$ treatment hardly affected the crystal structures compared with annealing in air, and Ba was still present as $BaZrO_3$ (Fig. 2C, $CO_2$).

TEM analysis of the $CO_2$-annealed catalysts with corresponding elemental mapping as shown in Fig. 5 confirmed these observations. For Pt/Ba/$CeO_2$, the $BaCO_3$ particles contained no discernible Ce from elemental mapping. Similar to the as-prepared material (Fig. 1), after $CO_2$ annealing, the $BaCO_3$ domains are still well mixed with the $CeO_2$ particles, which are larger due to sintering. In agreement with the XRD results for

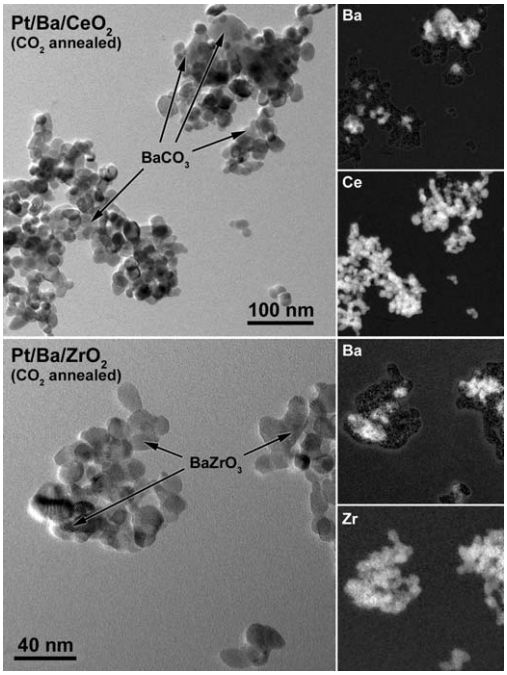


Fig. 5. TEM pictures of Pt/Ba on $CeO_2$ and $ZrO_2$ after annealing in $CO_2$ containing atmosphere. The corresponding elemental mappings of Ba, Ce, and Zr are shown on the left. $BaCO_3$ and $BaZrO_3$ domains are indicated by arrows.

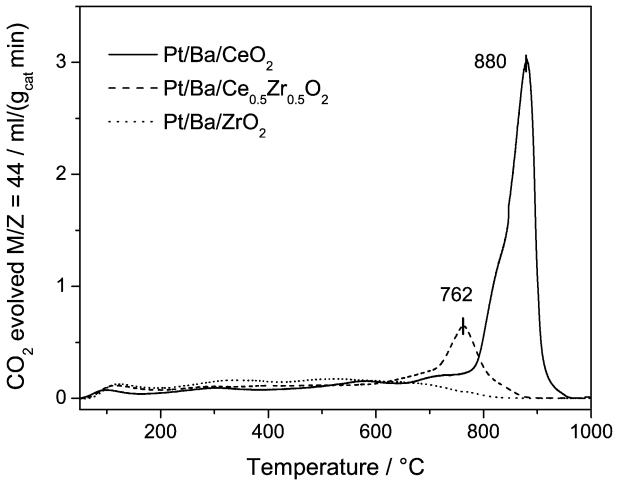


Fig. 6. TPD $CO_2$ evolution profiles during decomposition of $BaCO_3$ for $Pt/Ba/Ce_xZr_{1-x}O_2$ after annealing at 800 °C in 10% $O_2$/He (1 h) and 20% $CO_2$/He (1 h). Temperatures of maximum $BaCO_3$ decomposition rate are indicated.

$Pt/Ba/ZrO_2$ (Fig. 2C), elemental mapping revealed the presence of Zr in the Ba-containing domains, indicating the formation of $BaZrO_3$ at 800 °C. Interestingly, no distinct Pt particles or domains were observed by TEM (Fig. 5) or STEM analysis (not shown), indicating that no significant sintering occurred during annealing at 800 °C.

The TPD profiles recorded after $CO_2$ annealing further corroborate these results (Fig. 6). Recalling the $CO_2$ evolution from as-prepared materials (Fig. 3) it clearly shows the reformation of $BaCO_3$ on $CeO_2$. The amount of evolved $CO_2$ is even slightly higher than for the as-prepared $Pt/Ba/CeO_2$. This may be attributed to small amounts of BaO, $Ba(OH)_2$, or

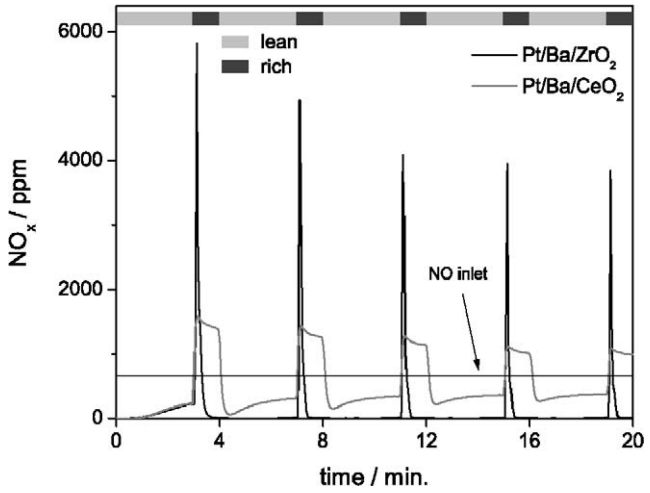


Fig. 7. $NO_x$ storage-reduction on as-prepared $Pt/Ba/ZrO_2$ and $Pt/Ba/CeO_2$ at 350. $NO_x$ concentration in the outlet gas is shown for the first 5 lean–rich cycles. After 3 min under lean atmosphere the gas composition was switch to rich conditions for 1 min and then changed back to lean. Pseudo steady-state was reached after four cycles.

$BaCeO_3$ in the as-prepared material, which are not detectable by XRD. These species then transform into $BaCO_3$ on treatment in $CO_2$. In addition, the maximum decomposition rate was shifted toward higher temperatures (880 instead of 840 °C), indicating the formation of larger $BaCO_3$ particles. On the other hand, on $Ce_{0.5}Zr_{0.5}O_2$, the $BaCO_3$ was only partly recovered in $CO_2$, and, consequently, less $CO_2$ evolved during TPD compared with the as-prepared material. Also in accordance with XRD, no $CO_2$ stemming from $BaCO_3$ decomposition was observed for $Pt/Ba/ZrO_2$ after $CO_2$ annealing, and only $CO_2$ desorbing from the surface at low temperatures was detected, indicating complete $BaZrO_3$ formation.

### 3.2. $NO_x$ storage-reduction

$Pt/Ba/Ce_xZr_{1-x}O_2$ catalysts were tested for their behavior in $NO_x$ storage and reduction. Fig. 7 depicts $NO_x$ outlet concentrations during five lean–rich cycles at 350 °C for catalysts supported on $CeO_2$ and $ZrO_2$. After 3 min under lean conditions (667 ppm NO, 6.67% $O_2$, He), the feed gas was abruptly switched to rich conditions (667 ppm NO, 1333 ppm $C_3H_6$, He) for 1 min and then back again. Interestingly, the $NO_x$ storage during the first cycle was similar for both catalysts; however, after that cycle, the catalyst was either activated or deactivated during the first three conditioning cycles, depending on the support. These differences are discussed later in this paper. Fig. 7 further shows that after an initial conditioning of the catalyst during cycles 1–3, near steady state was reached around the fourth cycle. For later comparison of the catalysts, only the fifth cycle, when this pseudo-steady state was established, is considered.

For comparison, Fig. 8 shows the $NO_x$ outlet concentrations during the fifth lean–rich cycle at 350 °C for $Pt/Ba/Al_2O_3$ reference catalysts prepared by incipient wetness impregnation [27] and two-nozzle FSP [16]. In agreement with earlier observations by pulse thermal analysis [17], $NO_x$ is stored much faster

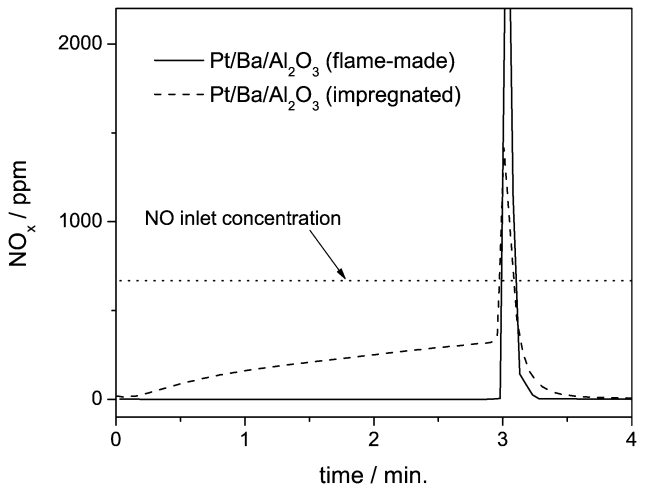


Fig. 8. $NO_x$ storage-reduction on reference $Pt/Ba/Al_2O_3$ catalysts prepared by flame synthesis and incipient wetness impregnation [17]. $NO_x$ outlet concentrations during the fifth lean–rich cycle at 350 °C are shown.

on the flame-made materials, resulting in no $NO_x$ breakthrough during the lean storage phase and higher $NO_x$ conversion, 91%, compared with 70% for the impregnated catalyst. This was attributed to the absence of thermally stable $BaCO_3$ (HT-$BaCO_3$) [17,27].

Fig. 9 depicts the corresponding the NO, $NO_2$, $NO_x$, and $CO_2$ outlet concentrations during the fifth lean–rich cycle at 350 and 400 °C for ceria–zirconia-supported catalysts. The lean-to-rich switch was accompanied by a sharp increase in $NO_x$. This breakthrough is commonly observed but not completely understood; proposed causes include (i) exothermic oxidation of $C_3H_6$ resulting in the fast release of $NO_x$, which is not completely reduced [34,35]; (ii) unselective reduction of released $NO_2$ into NO on $PtO_x$ sites before reduction of $PtO_x$ to $Pt^0$ under rich conditions, which is more selective toward $N_2$ [36]; and (iii) partial mixing of $O_2$ and $C_3H_6$, resulting in combustion and formation of a high amount of $CO_2$ which promotes $NO_x$ release [37] that is not reduced as long as $C_3H_6$ has been burnt off by $O_2$. For all of these experiments, the amount of $NO_2$ in the off-gas was very low (<20 ppm), with sharp peaks occurring only during the lean–rich switches. Distinct differences in storage and reduction behavior were found depending on the reactor temperature and the support composition.

At 350 °C complete reduction of $NO_x$ by $C_3H_6$ was achieved only for Zr-rich supports, whereas $NO_x$ was not reduced on $CeO_2$ and $Ce_{0.5}Zr_{0.5}O_2$, resulting in high $NO_x$ concentrations. The $ZrO_2$-supported catalyst exhibited similar storage and reduction behavior at 350 °C as the flame-made $Al_2O_3$-supported catalyst (Fig. 8). Increasing the temperature to 400 °C facilitated $NO_x$ reduction on the Ce-rich supports as well. After an initially fast $NO_x$ uptake on $Pt/Ba/CeO_2$ at 350 °C during the first 2 cycles, only low amounts of $NO_x$ were stored during the subsequent cycles (Fig. 7). This can be attributed to the presence of occupied storage sites formed during the previous cycles [35,38,39]. Because little or no $CO_2$ was formed through oxidation of $C_3H_6$, $Ba(NO_3)_2$ was not completely transformed back into $BaCO_3$, and the previously formed $Ba(NO_3)_2$ survived the rich phase, blocking active storage sites during the

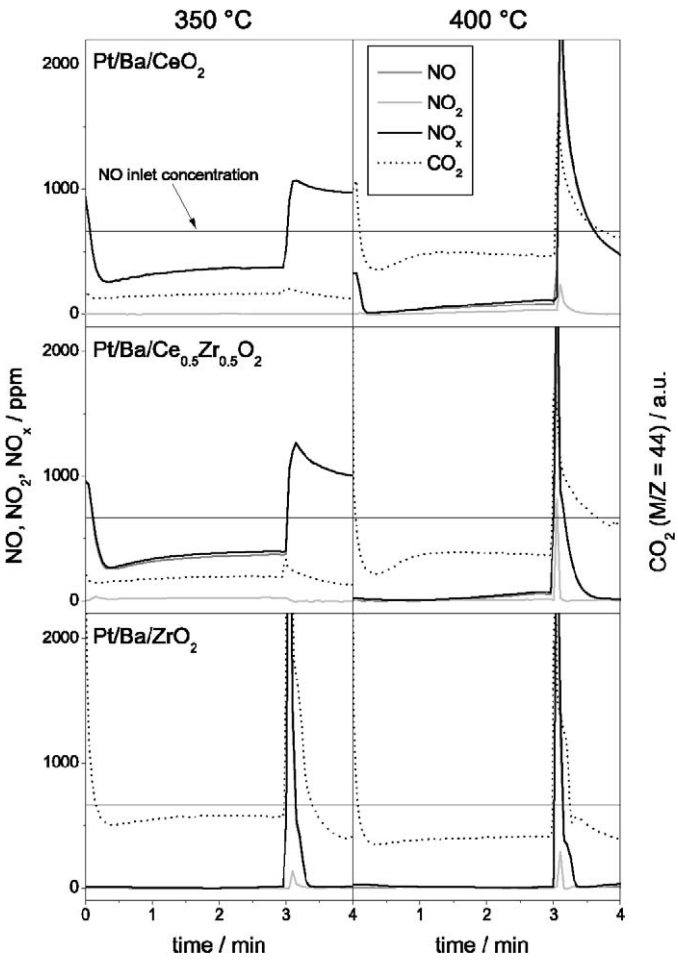


Fig. 9. $NO_x$ storage-reduction on as-prepared $Pt/Ba/Ce_xZr_{1-x}O_2$ with different support composition at 350 and 400 °C. Effluent gases (NO, $NO_2$, $NO_x$, and $CO_2$) are shown during the fifth lean–rich cycle. After 3 min under lean atmosphere the gas composition was switched to rich conditions for 1 min.

subsequent lean phases. Complete storage experiments (as discussed later) and $CO_2$ traces corroborate these assumptions and further show that $NO_x$ storage is always accompanied by $CO_2$ evolution from $BaCO_3$, the active form of Ba in the storage process.

Fig. 10 shows the $NO_x$ conversion on $Pt/Ba/Ce_xZr_{1-x}O_2$ during the fifth lean–rich cycle at different temperatures. Independent of support composition, the $NO_x$ conversion was very low at 300 °C. As discussed before, this is due mainly to the low reduction activity of platinum at this low temperature. At 350 °C, however, the higher reduction activity strongly increased the $NO_x$ conversion, but only for catalysts containing little or no Ce in the support. For Ce:Zr ratios >1, the conversion was still very low. At even higher temperatures (400 °C), all catalysts reduced $NO_x$ during rich phases (Fig. 9), resulting in high $NO_x$ conversion.

Figs. 9 and 10 clearly show the negative influence of ceria on the reduction activity of Pt and consequently on $NO_x$ conversion. Similar observations have been made for NO reduction by $CH_4$ or $C_3H_6$ on $Pt/Ce_xZr_{1-x}O_2$ [40,41]. The low activity with $CeO_2$-rich supports can be attributed either to the inhibition caused by the release of oxygen from $CeO_2$ during

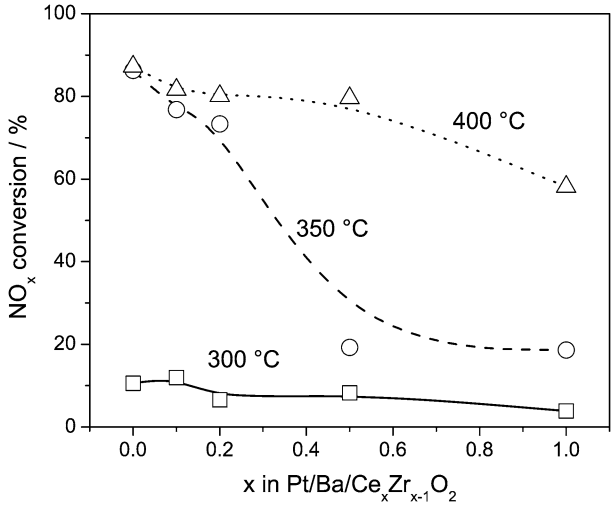


Fig. 10. $NO_x$ conversion as a function of temperature and support composition during the fifth lean–rich cycle (compare Fig. 7).

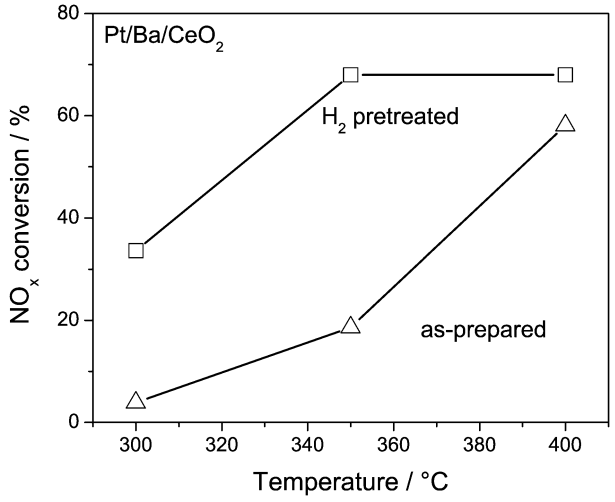


Fig. 11. $NO_x$ conversion during the fifth lean–rich cycle for as-prepared Pt/Ba/$CeO_2$ and after $H_2$ pretreatment (5% $H_2$/Ar, 500 °C, 30 min) as a function of temperature.

rich phases or to the formation of platinum oxides, which are less active. The formation of very stable $PtO_x$ on flame-made $Ce_{0.5}Zr_{0.5}O_2$ has been reported previously [19]. In that study, a temperature of 300 °C was needed for complete reduction of $PtO_x$ (1 wt% Pt) in 5% $H_2$. The small size of Pt particles together with $PtO_x$ stabilization by ceria results in the high stability of Pt in its oxidized form [19,40]. Here, the presence of predominantly $PtO_x$ or $Pt^0$ was indicated by an orange/brown or gray powder color, respectively. As-prepared materials on Ce-rich supports exhibited an orange/brown color, whereas the as-prepared Pt/Ba/$ZrO_2$ was light gray. In agreement with earlier observations [19], the color of the powders turned dark gray around 300 °C upon reduction in 5% $H_2$, indicating the formation of $Pt^0$. During reaction, the observed color changes were in good agreement with the corresponding NSR activity; that is, for Ce:Zr >1, the orange color (predominantly $PtO_x$) was retained at 350 °C even for long rich periods, but at 400 °C, along with a strongly increased activity, these materials turned

Table 1
NSR activity for as-prepared, $CO_2$ annealed and $H_2$ pretreated Pt/Ba/$CeO_2$ and Pt/Ba/$ZrO_2$ catalysts

| Sample | Annealing[a] | $T$[b] (°C) | $NO_x$ conversion[c] (%) |
|---|---|---|---|
| Pt/Ba/$CeO_2$ | None | 400 | 58.1 |
| | A | 400 | 11.7 |
| | B | 300 | 33.6 |
| Pt/Ba/$ZrO_2$ | None | 400 | 87.1 |
| | A | 400 | 4.2 |
| | B | 300 | 52.8 |

[a] A: 1 h at 800 °C in 10% $O_2$/He followed by 1 h in 20% $CO_2$/He; B: 5% $H_2$/Ar, 500 °C, 30 min.
[b] Temperature during $NO_x$ storage-reduction measurement.
[c] $NO_x$ conversion during fifth lean–rich cycle.

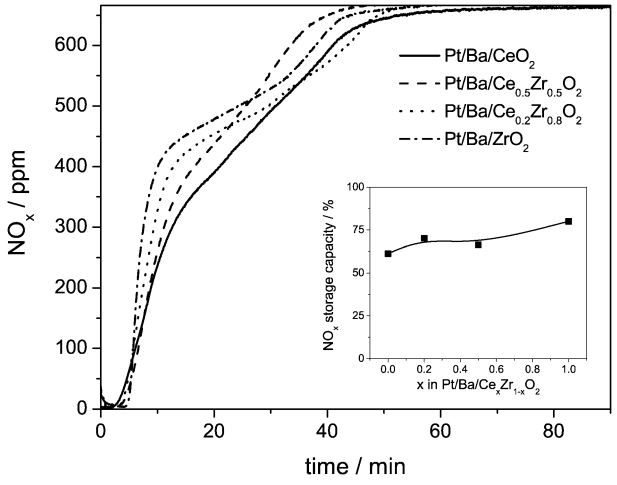


Fig. 12. $NO_x$ outlet concentration during saturation experiments at 400 °C after 5 lean–rich cycles for Pt/Ba/$Ce_xZr_{1-x}O_2$. The inset depicts the corresponding $NO_x$ storage capacity as derived from the stored $NO_x$.

gray, indicating the formation of active $Pt^0$. The higher activity of Zr-rich catalysts can thus be attributed to easier reducible $PtO_x$ species. NSR experiments with prereduced catalysts further corroborate these findings.

Fig. 11 shows the $NO_x$ conversion of as-prepared and prereduced Pt/Ba/$CeO_2$. Reduction of Pt at 500 °C in 5% $H_2$/Ar before the experiments strongly enhanced the $NO_x$ reduction activity of Pt at lower temperatures and thus increased the corresponding $NO_x$ conversion. Even at 300 °C, the prereduced Pt was active for $NO_x$ reduction, resulting in a $NO_x$ conversion of 33.6%. The hydrogen pretreatment also increased the $NO_x$ reduction activity for Pt on $ZrO_2$, resulting in a $NO_x$ conversion of 52.8% at 300 °C compared with 10.6% for the as-prepared material (Table 1, Fig. 10).

Fig. 12 depicts the $NO_x$ outlet concentrations from Pt/Ba on four supports during complete storage until saturation at 400 °C measured after five lean–rich cycles. No breakthrough of $NO_x$ was observed for about 5 min. After 5 min, the $NO_x$ concentration increased rapidly but did not reach the inlet concentration, indicating that $NO_x$ is still partly stored for another 50 min. These results show two different $NO_x$ storage activities of the catalysts: a fast $NO_x$ uptake during a first period with all $NO_x$ being stored, followed by a slower process with only

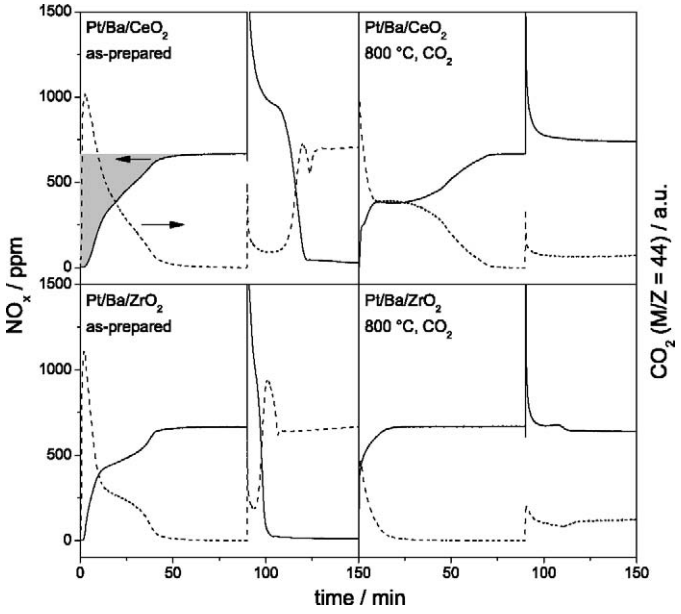


Fig. 13. $NO_x$ and $CO_2$ in the effluent gas during NSR on $Pt/Ba/CeO_2$ and $Pt/Ba/ZrO_2$, as-prepared and after annealing in $CO_2$ containing atmosphere. The catalysts were exposed to lean conditions until saturation (90 min) followed by reducing conditions for 45 min. The gray area indicates the amount of stored $NO_x$ (compare Table 2).

partial storage of $NO_x$. The first, fast process contributes approximately 15–20% to the total amount of stored $NO_x$. The reason for these different rates cannot be attributed to different storage activities of BaO or $BaCO_3$, because $CO_2$ evolved corresponding to the amount of $NO_x$ stored (compare Fig. 13). This demonstrates that only $BaCO_3$ was the active storage component.

Another explanation for the different storage rates is much more plausible. During the first period, $NO_x$ rapidly reacts on the surface of the $BaCO_3$ particles, forming a $Ba(NO_3)_2$ surface layer. Once the surface is saturated, the slower storage process starts. Now the nitrates or $NO_2$ have to diffuse into the particles and carbonates or $CO_2$ to the surface, where they can be released. Compared with the fast surface reaction, this diffusion process is slower limiting the $NO_x$ uptake rate during the second period. This mechanism has been proposed for $Pt/Ba/Al_2O_3$ and also evaluated by modeling approaches [35, 38,39]. We observed this behavior for all support compositions; however, on supports with high Ce content, the second diffusion process occurred faster. The inset in Fig. 12 shows the corresponding $NO_x$ storage capacities as a function of support composition expressed in terms of percentage of Ba involved in the storage process assuming complete $Ba(NO_3)_2$ formation. For all catalysts, the $NO_x$ storage capacity was rather high (>60%) and increased with higher Ce content up to 80%.

The NSR activity of $Pt/Ba/Ce_xZr_{1-x}O_2$ was also tested after thermal decomposition and recovery of $BaCO_3$ in $CO_2$ containing atmosphere. Table 1 depicts the corresponding $NO_x$ conversion at 400 °C during the fifth lean–rich cycle for as-prepared and annealed catalysts. On both supports ($CeO_2$ and $ZrO_2$), NSR activity decreased dramatically after annealing. This is not surprising for $Pt/Ba/ZrO_2$, because no active $BaCO_3$ was

Table 2
Amount of stored $NO_x$ and relative amount of Ba involved in the storage process during saturation experiments at 400 °C (compare Fig. 10)

| Sample | Annealing[a] | $NO_x$ stored (mg $g_{cat}^{-1}$) | $NO_x$ storage capacity[b] (%) |
|---|---|---|---|
| $Pt/Ba/CeO_2$ | No | 51.8 | 77 |
| | Yes | 62.2 | 92 |
| $Pt/Ba/Ce_{0.5}Zr_{0.5}O_2$ | Yes | 32.5 | 48 |
| $Pt/Ba/ZrO_2$ | No | 40.9 | 61 |
| | Yes | 6.6 | 10 |

[a] 1 h at 800 °C in 10% $O_2$/He followed by 1 h in 20% $CO_2$/He.
[b] Relative amount of Ba involved in storage process, assuming complete $Ba(NO_3)_2$ formation.

recovered during the $CO_2$ treatment and only inactive $BaZrO_3$ was present (see Fig. 2). However, although $BaCO_3$ was reformed on $CeO_2$, rather low $NO_x$ conversions were observed. Additional experiments investigating the $NO_x$ storage capacity without any previous NSR cycles gave more insight into the behavior of as-prepared and $CO_2$ annealed catalysts.

Fig. 13 depicts the $NO_x$ and $CO_2$ outlet concentrations during saturation experiments at 400 °C without any previous lean–rich cycles for as-prepared and annealed catalysts. Corresponding $NO_x$ storage capacities are shown in Table 2. On as-prepared materials $NO_x$ uptake and storage capacities are similar to those after lean–rich cycles (Fig. 12). However, only on $ZrO_2$ the reduction activity was retained after saturation and complete transformation of $BaCO_3$ into $Ba(NO_3)_2$. Much lower reduction activity was observed for as-prepared $Pt/Ba/CeO_2$ after switching to rich conditions resulting in a large breakthrough of $NO_x$. Note that the $NO_x$ outlet concentration is even higher than its inlet concentration. It took a long time (30 min) until the reduction activity was recovered and $NO_x$ was reduced completely. $CO_2$ evolution corroborates the low reduction activity of $Pt/Ba/CeO_2$ as no $CO_2$ was formed from $C_3H_6$ oxidation. Compared to the reduction behavior after short storage periods (Fig. 9) much lower reduction activity was observed after complete storage. This may be attributed to blocking of active Pt sites by newly formed $Ba(NO_3)_2$ dispersing over the support [42].

Regarding the corresponding storage behavior of annealed catalysts (Fig. 13), it is obvious that hardly any $NO_x$ is stored on $Pt/Ba/ZrO_2$, which exhibits very low $NO_x$ storage capacity after the high-temperature treatment (Table 2). This is a consequence of the absence of active Ba-containing species. Here Ba is present predominantly as inactive $BaZrO_3$ (compare Figs. 2C and 6). In contrast, the reformation of $BaCO_3$ from $BaCeO_3$ in $CO_2$-containing atmosphere recovers the $NO_x$ storage activity. The $NO_x$ storage capacity was even higher (92%) than for the as-prepared $Pt/Ba/CeO_2$ (77%), which is in line with larger amounts of $BaCO_3$ on the annealed material (compare Figs. 2 and 6). The diffusion-limited storage of $NO_x$ is more pronounced than for the as-prepared catalyst. This is in good agreement with the formation of larger $BaCO_3$ particles during the annealing procedure (compare Figs. 2 and 5), which exhibit less accessible surface $BaCO_3$ for fast $NO_x$ uptake. $BaCO_3$ was partly reformed on $Ce_{0.5}Zr_{0.5}O_2$; consequently, this mate-

rial recovered some of its $NO_x$ storage capacity after annealing (Table 2). However, independent of the support composition, the reduction activity of the annealed materials was completely lost. Neither stored $NO_x$ nor NO from the feed gas was reduced, and hardly any formation of $CO_2$ was visible during the rich period. This inactivity is also the reason for the low $NO_x$ conversion during short lean–rich cycles (Table 1). The reason for this deactivation is not yet clear. Strong sintering of Pt can be excluded, because no large Pt particles were found by TEM analysis (Fig. 5) and no crystalline Pt (which is characteristic of large Pt particles) could be detected by XRD after annealing. The reaction of Pt with the support and/or Ba seems to be a more feasible explanation for this deactivation. The formation of $Ba_2CePtO_6$ perovskite structures at high temperatures has been reported [43]. Although no reflections of such phases were found in the diffraction patterns (Fig. 2), it is still possible that Pt deactivates by incorporation into the Ba and/or support matrix. However, further investigations are needed to elucidate this deactivation of Pt at high temperatures.

## 4. Conclusion

Two-nozzle FSP has been applied for synthesis of Pt/Ba/$Ce_xZr_{1-x}O_2$ consisting of individual $BaCO_3$ and ceria/zirconia particles. The as-prepared catalysts exhibited a high $NO_x$ storage capacity, but high amounts of ceria in the support lowered the $NO_x$ reduction activity of Pt due to the formation of less active stable Pt oxides. The catalysts could be activated by a reductive pretreatment, resulting in the formation of more active $Pt^0$. When exposed to $CO_2$, active $BaCO_3$ could be recovered after $BaCO_3$ decomposition and $BaZrO_3$/$BaCeO_3$ formation at high temperatures. Complete $BaCO_3$ recovery could be achieved on $CeO_2$, whereas $BaCO_3$ was not reformed on $ZrO_2$ and only partly reformed on Ce–Zr mixed oxide. Pt was strongly deactivated during the annealing procedure, resulting in a loss of the catalyst's $NO_x$ reduction activity. Flame-made Pt/Ba/ceria–zirconia NSR catalysts are efficient for $NO_x$ storage; however, further investigations in the presence of real exhaust gases also containing $CO_2$, $H_2O$, and $SO_2$ are needed to finally assess the potential of flame-made Pt/Ba/ceria–zirconia for $NO_x$ storage. As concerns the reduction/oxidation behavior, it may be interesting to investigate the performance of other platinum group metals or bimetallic systems based on ceria–zirconia supports.

## Acknowledgments

We thank Dr. Marek Maciejewski and Maria Casapu (Institute of Chemical and Bioengineering) for their helpful suggestions. Financial support by the Swiss Federal Institute of Technology (ETH, TH 2/03-2) is kindly acknowledged.

## References

[1] N. Miyoshi, S. Matsumoto, K. Katoh, T. Tanaka, J. Harada, N. Takahashi, K. Yokota, M. Sugiura, K. Kasahara, SAE Technical Paper 950809, 1995.
[2] W. Bogner, M. Kramer, B. Krutzsch, S. Pischinger, D. Voigtlander, G. Wenninger, F. Wirbeleit, M.S. Brogan, R.J. Brisley, D.E. Webster, Appl. Catal. B Environ. 7 (1995) 153.
[3] S. Matsumoto, CATTECH 4 (2000) 102.
[4] E. Fridell, H. Persson, B. Westerberg, L. Olsson, M. Skoglundh, Catal. Lett. 66 (2000) 71.
[5] W.S. Epling, L.E. Campbell, A. Yezerets, N.W. Currier, J.E. Parks, Catal. Rev. 46 (2004) 163.
[6] S. Matsumoto, Y. Ikeda, H. Suzuki, M. Ogai, N. Miyoshi, Appl. Catal. B Environ. 25 (2000) 115.
[7] B.H. Jang, T.H. Yeon, H.S. Han, Y.K. Park, J.E. Yie, Catal. Lett. 77 (2001) 21.
[8] C. Courson, A. Khalfi, H. Mahzoul, S. Hodjati, N. Moral, A. Kiennemann, P. Gilot, Catal. Commun. 3 (2002) 471.
[9] F. Rohr, S.D. Peter, E. Lox, M. Kögel, A. Sassi, L. Juste, C. Rigaudeau, G. Belot, P. Gélin, M. Primet, Appl. Catal. B Environ. 56 (2005) 201.
[10] C. Sedlmair, K. Seshan, A. Jentys, J.A. Lercher, Res. Chem. Intermediat. 29 (2003) 257.
[11] S. Elbouazzaoui, E.C. Corbos, X. Courtois, P. Marecot, D. Duprez, Appl. Catal. B Environ. 61 (2005) 236.
[12] Z.Q. Liu, J.A. Anderson, J. Catal. 228 (2004) 243.
[13] H. Hirata, I. Hachisuka, Y. Ikeda, S. Tsuji, S. Matsumoto, Top. Catal. 16 (2001) 145.
[14] J.P. Breen, M. Marella, C. Pistarino, J.R.H. Ross, Catal. Lett. 80 (2002) 123.
[15] M. Casapu, J.D. Grunwaldt, M. Maciejewski, M. Wittrock, U. Göbel, A. Baiker, Appl. Catal. B Environ. 63 (2006) 232.
[16] R. Strobel, L. Mädler, M. Piacentini, M. Maciejewski, A. Baiker, S.E. Pratsinis, Chem. Mater. 18 (2006) 2532.
[17] M. Piacentini, R. Strobel, M. Maciejewski, S.E. Pratsinis, A. Baiker, J. Catal. 243 (2006) 82.
[18] R. Strobel, W.J. Stark, L. Mädler, S.E. Pratsinis, A. Baiker, J. Catal. 213 (2003) 296.
[19] W.J. Stark, J.D. Grunwaldt, M. Maciejewski, S.E. Pratsinis, A. Baiker, Chem. Mater. 17 (2005) 3352.
[20] A.C. Sutorik, M.S. Baliat, Mater. Sci. Forum 386 (3) (2002) 371.
[21] W.J. Stark, L. Mädler, M. Maciejewski, S.E. Pratsinis, A. Baiker, Chem. Commun. (2003) 588.
[22] J. Kaspar, P. Fornasiero, M. Graziani, Catal. Today 50 (1999) 285.
[23] M. Eberhardt, R. Riedel, U. Göbel, J. Theis, E.S. Lox, Top. Catal. 30–31 (2004) 135.
[24] L.F. Liotta, A. Macaluso, G.E. Arena, M. Livi, G. Centi, G. Deganello, Catal. Today 75 (2002) 439.
[25] V.G. Milt, C.A. Querini, E.E. Miro, M.A. Ulla, J. Catal. 220 (2003) 424.
[26] L. Mädler, W.J. Stark, S.E. Pratsinis, J. Mater. Res. 17 (2002) 1356.
[27] M. Piacentini, M. Maciejewski, A. Baiker, Appl. Catal. B Environ. 59 (2005) 187.
[28] W. Grogger, F. Hofer, P. Warbichler, G. Kothleitner, Microsc. Microanal. 6 (2000) 161.
[29] R. Mueller, R. Jossen, S.E. Pratsinis, M. Watson, M.K. Akhtar, J. Am. Ceram. Soc. 87 (2004) 197.
[30] R. Strobel, M. Maciejewski, S.E. Pratsinis, A. Baiker, Thermochim. Acta 445 (2006) 23.
[31] T. Nishino, T. Sakurai, N. Ishizawa, N. Mizutani, M. Kato, J. Solid State Chem. 69 (1987) 24.
[32] M. Piacentini, M. Maciejewski, T. Bürgi, A. Baiker, Top. Catal. 30–31 (2004) 71.
[33] W.J. Stark, M. Maciejewski, L. Mädler, S.E. Pratsinis, A. Baiker, J. Catal. 220 (2003) 35.
[34] K.S. Kabin, R.L. Muncrief, M.P. Harold, Catal. Today 96 (2004) 79.
[35] L. Olsson, E. Fridell, M. Skoglundh, B. Andersson, Catal. Today 73 (2002) 263.
[36] I. Nova, L. Castoldi, L. Lietti, E. Tronconi, P. Forzatti, Catal. Today 75 (2002) 431.
[37] A. Amberntsson, H. Persson, P. Engstrom, B. Kasemo, Appl. Catal. B Environ. 31 (2001) 27.
[38] R.L. Muncrief, P. Khanna, K.S. Kabin, M.P. Harold, Catal. Today 98 (2004) 393.
[39] U. Tuttlies, V. Schmeisser, G. Eigenberger, Top. Catal. 30–31 (2004) 187.

[40] L.F. Liotta, A. Longo, A. Macaluso, A. Martorana, G. Pantaleo, A.M. Venezia, G. Deganello, Appl. Catal. B Environ. 48 (2004) 133.
[41] R. Perez-Hernandez, F. Aguilar, A. Gomez-Cortes, G. Diaz, Catal. Today 107–108 (2005) 175.
[42] J. Szanyi, J.H. Kwak, J. Hanson, C.M. Wang, T. Szailer, C.H.F. Peden, J. Phys. Chem. B 109 (2005) 7339.
[43] K. Ouchetto, F. Archaimbault, A. Pineau, J. Choisnet, J. Mater. Sci. Lett. 10 (1991) 1277.